iScience

Article

Reprogramming the melanoma and immunosuppressive myeloid cells with esomeprazole-loaded PLGA nanoparticles

Graphical abstract

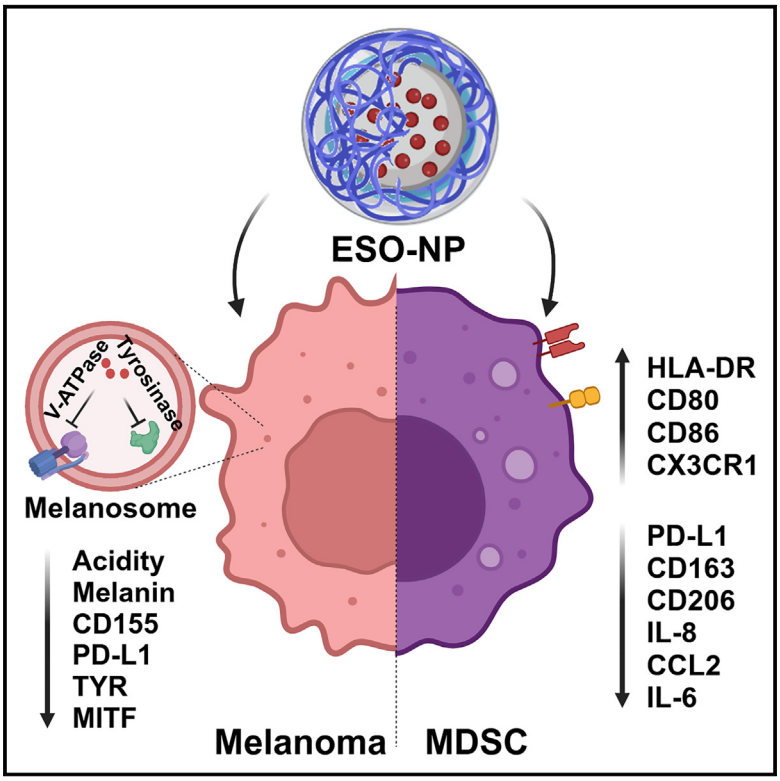

Highlights

- Stable core-shell PLGA nanoparticles with esomeprazole cargo (ESO-NP) are developed
- ESO-NPs modulate intracellular pH, affecting immune checkpoint expression in melanoma
- ESO-NPs alter HLA-DR and PD-L1 in induced and melanoma patient myeloid-derived suppressor cells (MDSCs)
- ESO-NPs can potentially reduce resistance to cancer therapy and immune suppression

Authors

Nicola Cerioli, Wissem Bououdina, Alessandro Mereu, ..., Carl G. Figdor, Veronica Huber, Oya Tagit

Correspondence

veronica.huber@istitutotumori.mi.it (V.H.), oya.tagit@fhnw.ch (O.T.)

In brief

Biological sciences; Biotechnology; Immunology; Medical biotechnology

Cerioli et al., 2025, iScience *28*, 111559
January 17, 2025
https://doi.org/10.1016/j.isci.2024.111559

CellPress

iScience

CellPress
OPEN ACCESS

Article

Reprogramming the melanoma and immunosuppressive myeloid cells with esomeprazole-loaded PLGA nanoparticles

Nicola Cerioli,[1,6] Wissem Bououdina,[2,4,6] Alessandro Mereu,[1,6] Evangelos Natsaridis,[3] Jeannette Salsetta,[1] Agata Cova,[1] Gianpiero Lupoli,[1] Elisa D'Angelo,[1] Licia Rivoltini,[1] Carl G. Figdor,[2] Veronica Huber,[1,7,8,*] and Oya Tagit[2,3,5,7,*]

[1]Translational Immunology Unit, Fondazione IRCCS Istituto Nazionale dei Tumori, Milan, Italy
[2]Department of Tumor Immunology, Radboud Institute for Molecular Life Sciences, Radboud University Medical Center, Nijmegen, the Netherlands
[3]Group of Biointerfaces, Institute of Chemistry and Bioanalytics, School of Life Sciences FHNW, Muttenz, Switzerland
[4]Present address: MRC Protein Phosphorylation and Ubiquitylation Unit, University of Dundee, Dundee, UK
[5]Present address: Swiss Nanoscience Institute, University of Basel, Basel, Switzerland
[6]These authors contributed equally
[7]Senior author
[8]Lead contact
*Correspondence: veronica.huber@istitutotumori.mi.it (V.H.), oya.tagit@fhnw.ch (O.T.)
https://doi.org/10.1016/j.isci.2024.111559

SUMMARY

Proton pump inhibitors have been explored for potentiating cancer therapies via reverting the tumor acidity and promoting the activation of anti-tumor immune responses. To regulate the intracellular pH of melanoma and immunosuppressive myeloid cells, we developed poly(L-lactide-co-glycolide) nanoparticles loaded with esomeprazole (ESO-NPs). The effect of ESO-NPs on melanoma cells was observed as alkalinization and reduction of melanin content accompanied by a decrease of microphthalmia-associated transcription factor (MITF), poliovirus receptor (PVR), and programmed death ligand 1 (PD-L1) immune checkpoint expression. ESO-NP treatment of melanoma-patient-derived and *in vitro*-induced myeloid-derived suppressor cells (MDSCs) reduced the expression of immunosuppression-associated molecules PD-L1, CD206, and CD163 on patient-derived myeloid cells while inducing the expression of co-stimulatory molecule CD86 and HLA-DR in the *in vitro* model. Our findings suggest that reprogramming the intracellular pH of melanoma and immune-suppression-associated myeloid cells with ESO-NPs can modulate the expression of proteins involved in resistance to cancer therapy and immunosuppression, thus potentially improving the response to immunotherapies.

INTRODUCTION

pH regulation is essential for cells to maintain various cellular and physiological functions. Disruption or impairment of pH balance has been implicated for several pathological conditions, such as cancer. The altered metabolic pathways associated with the increased glucose metabolism and elevated lactate production results in the accumulation of acidic metabolites in the extracellular space.[1] Melanoma cells can sustain proliferation and evade apoptosis under such acidic extracellular pH (pH_e) by maintaining intracellular pH (pH_i) above 7.2[2] through up-regulation of proton transporters, which are channels and/or pumps affecting the H^+ concentration on the two sides of the membrane.[3] These proton transporters—or proton pumps—also impact melanogenesis at different levels. According to melanosomal physiology, tyrosinase activity is pH dependent and melanin synthesis is reduced at low pH, consistent with more acidic melanosomes of fair-skinned individuals.[4] The pH of melanosomes changes from very acidic in early to neutral in late-stage maturation. Neutral pH is fundamental for optimal activity of the melanin synthesizing enzyme tyrosinase, and its activity is orchestrated by the balance of positive (increase pH) and negative (decrease pH) pH regulators. The blockage of proton pumps using proton pump inhibitors (PPIs) affects melanogenesis by inhibiting tyrosinase maturation and promoting its degradation through interference with ATP7A, a copper transporting P-type ATPase necessary for copper acquisition by tyrosinase. Prevention of copper transport causes hypopigmentation.[5] A decrease of melanin formation can be induced also by the copper-chelating activities of certain PPIs.[6]

There has been interest in PPIs to potentiate cancer therapies via dysregulating pH_i or via decreasing the tumor acidity (pH_e) to promote the activation of anti-tumor immune responses[7,8] and the concomitant relief of immune suppression fostered by cancer-associated myeloid cells, including myeloid-derived

suppressor cells (MDSCs).[9,10] MDSCs are a major driver in cancer progression and resistance to immunotherapy with immune checkpoint inhibitors (ICIs). Due to their high plasticity and the numerous pathways exploited by these cells to blunt anti-tumor immunity, a drug specifically targeting MDSC functions is still elusive.

Nanocarrier-mediated delivery of drugs could contribute to the targeting of myeloid cells by exploiting their natural phagocytic activity to deliver PPIs, such as esomeprazole (ESO), to reprogram the tumor microenvironment (TME), relieve immune suppression, and support immunotherapy with ICIs.[11] Conversely, in tumors, the overexpressed proton pumps may also facilitate targeted therapies by acting as both drug targets for PPIs and as surface markers for recognition and delivery of cytotoxic drugs selectively to tumor cells.[12] Several preclinical studies and some clinical trials have investigated the potential exploitation of PPIs to revert tumor-driven acidification of the TME and the consequent immune suppressive effects on anti-tumor immunity and resistance to chemotherapy and immunotherapy with ICIs.[12–16] Furthermore, nanoparticle (NP)-assisted delivery of PPIs has been explored in cancer in combination with chemotherapeutics.[12,17] NPs co-loaded with PPIs and anticancer drugs demonstrated enhanced cytotoxicity in various cancer cell lines such as human liver adenocarcinoma, human glioblastoma, and human pancreatic carcinoma.[17] In addition, pre-treatment of tumor-bearing mice with PPIs has been shown to substantially increase the circulation times and tumor accumulation of subsequently administered nanomedicines via preventing the capture of nanomedicines by the mononuclear macrophage system.[18]

Indeed, NP-based delivery can provide several benefits such as stability, retention, and targeted release of PPIs while avoiding systemic off-target effects. This may be particularly relevant for targeting purposes of MDSCs, which are major feeders of immune suppressive circuits and mechanisms of resistance to cancer therapies and are characterized by strong internalization activities.[19,20] Furthermore, NPs can deliver molecules to their intracellular targets, which otherwise cannot easily penetrate through membranes. Therefore, NP-based delivery can offer the unique ability to selectively modulate intracellular targets and compartments.

Poly(L-lactide-co-glycolide), PLGA, and NPs are among the most convenient drug delivery systems due to the high versatility, tunable degradation characteristics, and long clinical history of PLGA, which is a biocompatible and biodegradable polymer that has been approved for several therapeutic applications.[21–26] Previous studies reported PPI-loaded PLGA NPs (namely lansoprazole-PLGA NPs) for both acid suppression in gastrointestinal ulcers[27] and reverting the paclitaxel resistance in tumor cells.[28] Despite the advantages that NP-based delivery of PPIs can offer, to the best of our knowledge, no studies have been reported on the modulation of pH_i of melanoma and immunosuppressive myeloid cells with PPI-loaded NPs, which could help reveal new mechanisms that affect melanoma metastasis or therapeutic response.

In this study, we developed PLGA NPs loaded with ESO to modulate the intracellular pH of different melanoma cell lines, namely 501 mel, LM38, LM47, and LM56. ESO is considered to be one of the most potent PPIs due to its unique molecular structure that enhances its inhibitory effect.[29,30] Its prolonged half-life compared to other PPIs facilitates sustained acid suppression. However, incorporating ESO into PLGA nanoparticles (ESO-NPs) poses several challenges due to the acid-labile nature of the drug and its interactions with the polymer. We customized the formulation parameters via the selection of appropriate stabilizers and solvents, which have a direct impact on the NP physicochemical characteristics, loading, and stability of drug, as well as the actual drug release profile.[31–34] In addition, we tested if ESO-NPs could reverse immune suppressive features of myeloid cells derived from peripheral blood of melanoma patients or immunosuppressive myeloid cells generated *in vitro*. Our results demonstrate that the physicochemical properties of ESO demand a particular core-shell nanoparticle structure for optimal encapsulation and retention stability. We observed that ESO-NPs were readily taken up by melanoma cells[35–37] and efficiently alkalinized intravesicular compartments, whereas the "free" ESO did not exert such effects. The modulation of melanoma cell pH_i also showed correlation with the surface expression of programmed death ligand 1 (PD-L1), suggesting that ESO-NPs can help revert acidification-driven immune suppressive effects. We could further observe these effects also with ESO-NP-treated MDSCs both derived from melanoma patients and *in vitro* generated, which lost their immune suppressive traits in terms of PD-L1, CD206, and CD163 expression, while inducing their activation in terms of co-stimulatory molecules and HLA-DR expression. Our results highlight various potential implications of ESO-NPs for cancer therapy including reduced resistance to chemotherapy and improved response to immunotherapy.

RESULTS AND DISCUSSION

Preparation of ESO-loaded PLGA nanoparticles

PLGA NPs are highly versatile platforms for the encapsulation and delivery of various compounds. Depending on the physicochemical properties of the cargo, single or double emulsions as well as nanoprecipitation techniques are commonly used. Stabilizers and surfactants are integral components of PLGA NPs with a direct influence on polymer-drug interactions that determine drug loading, stability, and release patterns.[33] PPIs are typically weak bases,[38] which can catalyze the hydrolysis of ester bonds, accelerating PLGA chain degradation and drug release. Basic drugs may also interfere with the polymer degradation by shielding the terminal carboxyl residues, thereby slowing down the degradation process by limiting the autocatalytic degradation of PLGA at low pH.[32] Therefore, preparation of stable ESO-loaded PLGA NPs requires a thorough consideration and investigation of different solvents and stabilizers to avoid drug-induced polymer degradation.

For the encapsulation of ESO, we used a double-emulsion method. Briefly, an aqueous solution of ESO was emulsified with the organic phase containing PLGA to form the primary emulsion, which was then mixed and sonicated with an aqueous solution of surfactant (PVA). This method results in the formation of a solid polymer matrix, through which the encapsulated drug molecules are distributed uniformly (Figure 1A). Several batches

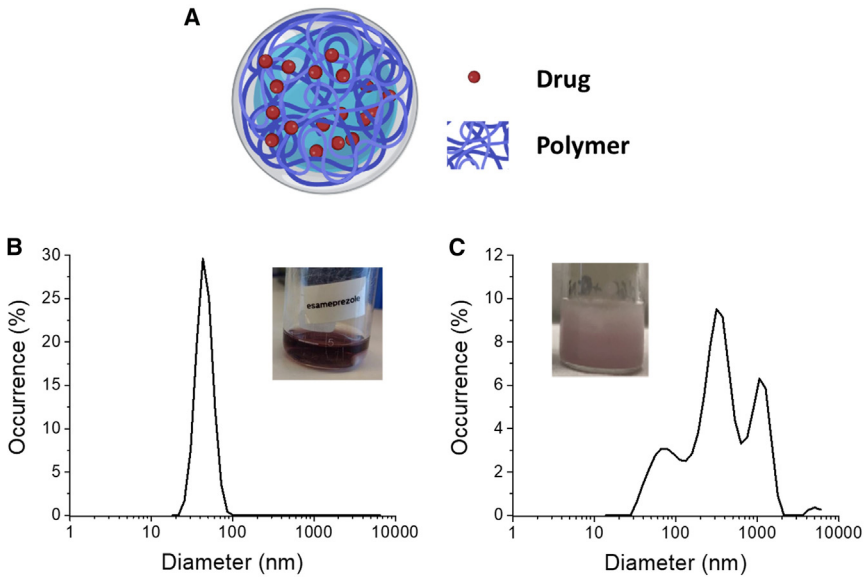

Figure 1. Failed batches of solid sphere ESO-NPs due to polymer-drug interactions

(A) Schematic presentation of drug-loaded PLGA NPs as a solid polymer matrix.

(B) The size distribution of ESO-NPs obtained when ESO solution was prepared in ultrapure water. Inset shows the dark purple color of the NP suspension.

(C) The size distribution of ESO-NPs obtained when ESO solution was prepared in borate buffer pH 10. Inset shows the pink-purple color of the NP suspension.

were produced, in which the aqueous ESO solution was prepared in various buffers as well as in ultrapure water to form the primary emulsion. The NP suspension obtained after overnight solvent evaporation was dark purple in color with an average size of 40 nm when ESO was dissolved in ultrapure water (Figure 1B). The observed color change indicated that ESO was likely being degraded, and the degradation products have possibly interfered with the formation of the PLGA nanoparticles. A similar color change observed for omeprazole solution was attributed to the degradation of drug in acidic environments (pH 3.0–4.0), leading to a dark purple-colored solution.[39] Chemically, ESO and omeprazole are identical except that omeprazole contains S and R stereoisomers, whereas ESO comprises only the S isomer. Therefore, an acidity-driven degradation could play a role in our experiments as the measured pH of purple suspension in Figure 1B was 5.5. As reported by Gul et al.,[40] ESO has a pK_a value of 9.68. To test whether dissolving ESO in a buffer with pH $\geq$ 10 would improve its stability and facilitate NP formation, we prepared ESO solution in borate buffer pH 10 (Figure 1C) and pH 11 as the dispersed phase of the primary emulsion. However, following the evaporation of organic solvent, an almost clear suspension with a pinkish hue was obtained in both cases. The yield of these batches were very poor ($\sim$5% of empty NPs prepared using the same method), and DLS measurements showed a highly polydisperse population with multiple peaks (Figure 1C). Therefore, we investigated the possible causes of drug degradation and failure of NP formation.

In our experiments, the degradation of ESO may have been caused by the drug-solvent, drug-surfactant, or drug-polymer interactions. To determine which component was responsible for the degradation of the ESO-NPs, we prepared a series of suspensions/emulsions. The aqueous solutions of ESO prepared in ultrapure water, PBS (pH 7.4), and borate buffer (pH 10 and 11) retained their yellowish tinge after overnight incubation. Next, a water solution of ESO was directly mixed with a 2% PVA solution, which remained clear and colorless. Following up, ESO was mixed directly with DCM and a turbid white suspension was obtained, which showed that ESO was stable but not soluble in DCM. Therefore, we concluded that the polymer-drug interactions were responsible for the degradation of ESO, as the reddish-purple precipitate was formed only in the presence of PLGA. Riedel and Leopold[41] reported that acidic groups in a polymer may lead to degradation of omeprazole, although to a lesser extent than monomeric acids. Furthermore, they showed that solution colors could vary from brown to dark red and purple based on the extent of degradation. Therefore, we focused on tailoring the nanocarrier structure to shield ESO from PLGA and minimize ESO-PLGA interactions.

Preparation of esomeprazole-loaded core-shell PLGA nanoparticles

The NPs that have been described so far were solid spheres, whose polymeric chains formed a matrix to entrap drugs. NPs can also be designed as vesicular nanostructures with a liquid inner core and a polymeric outer shell (Figure 2A).[42] This core-shell structure can improve the stability of ESO entrapped in the core, prevent polymer-drug interactions, and facilitate the formation of stable NPs. The core-shell NPs were formed by using sodium cholate as the stabilizer, which was exchanged with PVA after the evaporation of the organic solvent. Unlike the non-ionic PVA, sodium cholate is a small anionic surfactant with a bi-planar active surface: α-polar surface and β-hydrophobic surface.[43] Facing the hydrophilic core with the α surface and restricting the hydrophobic polymer on the β surface, these well-separated planes of sodium cholate can facilitate the formation of a core-shell structure and prevent or minimize the physical interactions between ESO and PLGA. Indeed, we obtained spherical ESO-loaded core-shell NPs (Figure 2B) with a narrow size distribution (intensity-averaged size: 173 nm, PDI: 0.06, black curve in Figure 2C), which did not show any noticeable color change, indicating the stability of ESO within the NP core. Empty core-shell PLGA NPs that were prepared in parallel displayed similar colloidal characteristics with an intensity-averaged size of 162 nm and a PDI of 0.05 (red curve in Figures 2C and S1). The size of the particles was within the desired range for cellular uptake (<200 nm), and the low PDI values (<0.2) indicated a monodisperse population. The Zeta potential of core-shell NPs were

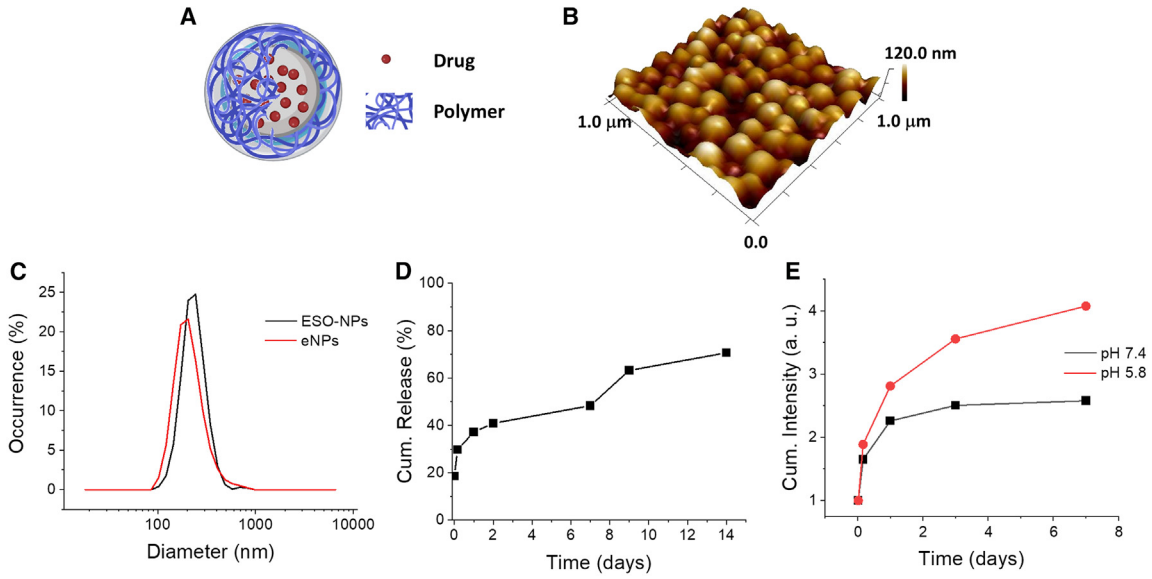

Figure 2. Colloidal characteristics and release profile of the ESO-loaded core-shell PLGA NPs

(A) Schematic illustration of ESO-loaded core-shell PLGA NPs.

(B) AFM image of ESO-loaded PLGA NPs. Scan size: 1 × 1 μm.

(C) Particle size distribution of ESO-loaded (black curve) and empty (red curve) core-shell PLGA NPs measured after re-suspension following lyophilization.

(D) Release profile of the ESO-loaded core-shell PLGA NPs obtained in PBS (pH 7.4) for a period of 14 days incubation at 37°C.

(E) Release profile of a fluorescent dye as a model drug obtained in PBS at pH 7.4 (black curve) and at pH 5.8 (red curve) for a period of 7 days incubation at 37°C.

−3.52 (±0.32) mV due to the non-ionic nature of surfactant (polyvinyl alcohol), which was used to exchange sodium cholate after the formation of core-shell nanoparticles.

Overall, the optimum formulation was obtained when ESO was dissolved in borate buffer pH 11 and sodium cholate was used as the surfactant. All the following characterizations and *in vitro* studies were implemented using this core-shell nanoformulation.

Next, we quantified the ESO content of the NPs by UV-Vis spectrometry. Absorbance values recorded at 301 nm were used for the calculation of drug encapsulation based on a calibration curve constructed with known ESO concentrations. ESO content per mg NP (determined as an average of two separately prepared batches) was 14.3 (±2.7) μg per mg particles, which corresponded to an approximately 10% encapsulation efficiency (9.9 ± 1.3%) and 1.43 (± 0.27) % drug loading. The release profile of the ESO-loaded core-shell PLGA NPs was studied *in situ* using absorption measurements. The particles were resuspended in PBS, then incubated at 37°C under constant agitation. At specific time points, the particles were pelleted, and the supernatant was collected to quantify the release over a period of 14 days. Following an initial burst release of ~20%, the release profile of the NPs showed a sustained release over the next 14 days and reached a total release of 70% by the end of the release studies (Figure 2D). The initial burst release is associated with the water uptake and swelling of lyophilized particles and is purely driven by drug diffusion. On the other hand, the combined effect of diffusion and matrix erosion is observed on the release pattern from day 7. Since we aim to modulate the pH of acidic intracellular compartments, we performed release studies at pH 5.8 as well. To avoid accelerated degradation of ESO in acidic conditions, which could interfere with the measurements and obscure the results, we used a green fluorescent dye as a model drug. The release profiles of the fluorescent dye in PBS at physiological (pH 7.4) and acidic (pH 5.8) conditions are compared in Figure 2E (black and red curves for pH 7.4 and pH 5.8, respectively). Dye-loaded PLGA NPs incubated at 37°C under constant agitation were pelleted at specific time points, and the supernatant was collected to quantify the release using fluorescence spectroscopy. For a clear comparison, measured fluorescence intensities were normalized to 1 at the initial measurement point. In line with previous reports,[44] Figure 2E shows a more rapid release at pH 5.8 in comparison to pH 7.4. By day 7, the amount of released dye at pH 5.8 was almost double the amount released at pH 7.4. It should be noted that the release is expected to be much faster *in vitro* and *in vivo* as the colloidal integrity of NPs vary greatly in different physiological conditions.[25] In our previous study, we evaluated the colloidal stability and integrity of PLGA NPs *in situ*, *in vitro*, and *in vivo* using a Förster resonance energy transfer (FRET)-based approach. By following the energy transfer between a donor and acceptor dye pair co-loaded into PLGA NPs, we observed a complete loss of FRET at 72 h *in vitro* and at time points as early as 24 h post-administration *in vivo*, whereas energy transfer was retained for approximately 2 weeks *in situ.*[25] Therefore, we used 72 h of incubation time in the following *in vitro* experiments.

Empty, ESO-loaded, and fluorescently labeled PLGA NPs produced as lyophilized powder stocks were dissolved in saline solution at a concentration of 10 mg/mL for the subsequent *in vitro* studies.

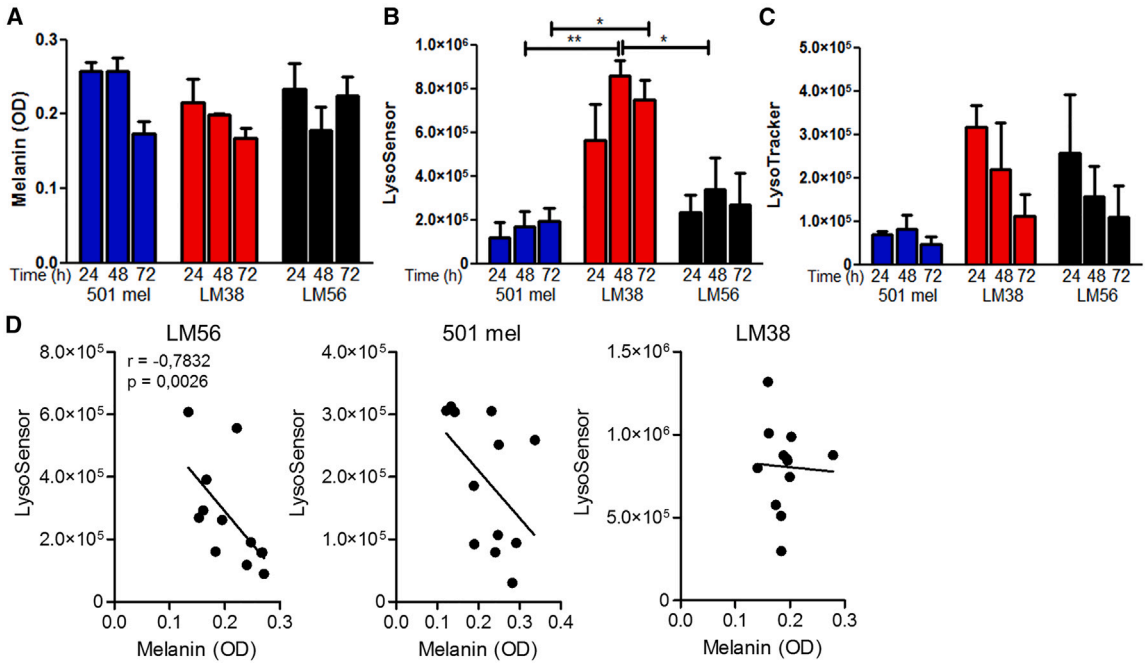

Figure 3. Basal features of melanoma cell lines

(A) Melanin quantification of 501 mel, LM56, and LM38, using UV-Vis spectrophotometer.

(B and C) LysoSensor and LysoTracker gMFI of the same cells. Shown are pooled results from three independent experiments at 24, 48, and 72 h of culture. Data are represented as mean ± SEM. Statistical significance was achieved by one-way ANOVA and Bonferroni's multiple comparison test ($p < 0.05$).

(D) Spearman correlation analysis of melanin content and LysoSensor levels. gMFI, geometric mean fluorescence intensity.

Basal features of melanoma cell lines

The experiments were conducted on melanoma cell lines 501 mel, LM56, and LM38. Among these, 501 mel is a wild-type melanoma cell line, whereas LM38 and LM56 present V600E mutation and LM38 cells display primary resistance to BRAF inhibitor PLX4032.[37] The cell lines displayed similar characteristics under basal culture conditions in terms of melanin content, which showed some fluctuation at 24, 48, and 72 h without reaching statistically significant difference (Figure 3A). However, the qualitative analysis of pH in the acidic organelles (including melanosomes) detected as LysoSensor levels revealed that LM38 cells displayed the highest LysoSensor geometric mean fluorescence intensity (gMFI), indicating a more acidic pH in intracellular compartments with respect to 501 mel and LM56 cell lines (Figure 3B). LysoSensor can help monitor fluctuations in pH due to its pH-dependent fluorescence intensity, which increases at low pH values. On the other hand, the fluorescence intensity of LysoTracker is independent of pH. It marks the acidic compartments, and the total fluorescence intensity is affected by the size, number, and content of the acidic organelles. The LysoTracker levels displayed a decreasing trend during the observation period and reached the lowest levels at the 72-h time point (Figure 3C), which could be associated with the continuous nutrient consumption during cell proliferation. Correlation analysis of collected results showed that the melanin content correlated negatively with LysoSensor levels, indicating that higher melanin levels were associated with less acidic pH, as expected. This was evident for LM56 and to a lesser extent for 501 mel cells, whereas LM38 cells did not show this association (Figure 3D).

Internalization of PLGA NPs by melanoma cells

To proceed with the ESO-NP treatment of melanoma cell lines, we first assessed their internalization activity using fluorescently labeled NPs (Atto647-NPs). LM38, LM56, and 501 mel cell lines were incubated with 20 and 100 μg/mL of Atto647-NPs, and their internalization was assessed by flow cytometry after 24, 48, and 72 h. These concentrations were chosen based on our experience with NP internalization dynamics by human cell lines. Of the different time points tested, the Atto647 gMFI showed an increase until 48 h and reached saturation at this time point. All three cell lines displayed a stronger internalization activity in the presence of 100 μg/mL Atto647-NPs compared to 20 μg/mL, suggesting that at the lower concentration of 20 μg/mL cells were not saturated by the internalization of the Atto647-NPs. Time-dependent internalization curves displayed a similar trend for both NP concentrations albeit at different Atto647 gMFI levels. Of note, LM38 cells, which are characterized by higher basal LysoSensor levels (Figure 3B), displayed the strongest internalization activity reflected by the highest Atto647 gMFI levels, whereas the other two melanoma cell lines showed more modest Atto647 gMFI values and similarity between each other (Figures 4A and 4B). The cells exposed to the Atto647-NPs were concomitantly evaluated for LysoSensor and LysoTracker levels by flow cytometry to verify if the internalization of PLGA NPs could impact intracellular acidity, as demonstrated

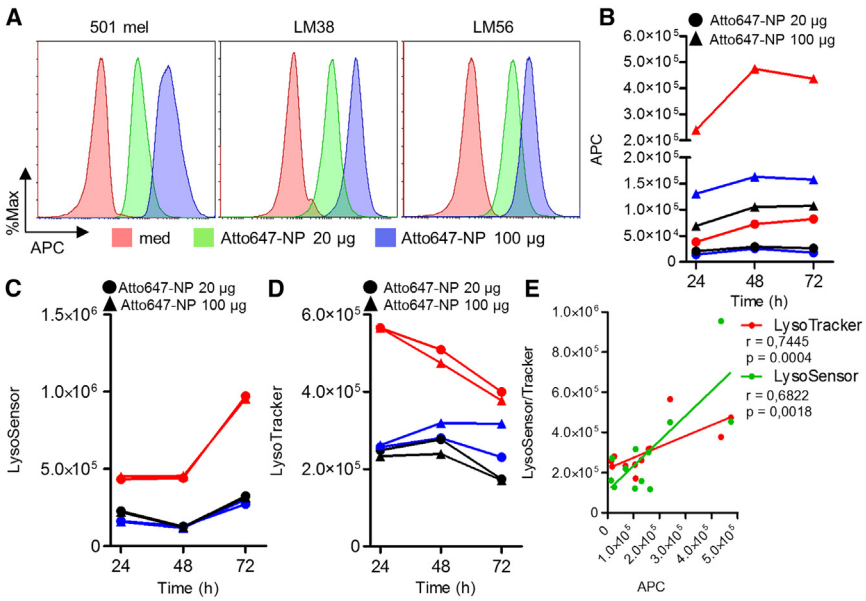

Figure 4. Internalization of PLGA NPs by melanoma cell lines

(A) NPs encapsulating Atto647 (Atto647-NPs) are internalized by melanoma cell lines.

(B) gMFI levels at 24, 48, and 72 h incubation of the cell lines incubated with 20 μg or 100 μg Atto647-NPs.

(C) gMFI levels of LysoSensor measured in cells during Atto647-NP internalization.

(D) gMFI levels of LysoTracker measured in cells during Atto647-NP internalization.

(E) Spearman correlation of Atto647 gMFI with LysoTracker and LysoSensor gMFI levels. Red dots and triangles LM38, blue dots and triangles 501 mel, black dots and triangles LM56 cells. gMFI, geometric mean fluorescence intensity.

by other groups.[45] Regardless of the concentration, the internalization of PLGA NPs was associated with intracellular pH variations (Figure 4C), which could be related to the degradation of PLGA NPs into glycolic acid and lactic acid,[46] leading to an increase of intracellular acidity as evidenced by higher LysoSensor levels at 72 h. On the other hand, LysoTracker measurement (Figure 4D) exhibited a trend similar to what we observed in the absence of NPs (Figure 3C). Nonetheless, the significant correlation of the Atto647-APC gMFI, especially with LysoTracker levels, indicated PLGA internalization within the acidic organelles of melano/endosomal compartments (Figure 4E).

Effect of esomeprazole-loaded PLGA NPs on melanoma cells

We next investigated the delivery, internalization, and biological activity of the PPI esomeprazole-loaded PLGA NPs (ESO-NP) on melanoma cell lines. Based on previous studies[5] and results shown in Figure 4, we chose the 72 h time point to test ESO-NP activity. The treatment of the three melanoma cell lines with NPs containing 1 μg ESO-NP or empty NPs (eNPs) revealed a decrease of LysoSensor values, which was particularly evident for 501 mel and LM56 cells, with respect to eNP (Figure 5A). The melanoma cell line LM38 displayed a −12.19% gMFI LysoSensor shift in comparison to eNPs, whereas the gMFI of LM56 and 501 mel displayed a shift of −53.12% and −90.33%, respectively. Our results suggest a decrease of intracellular acidity of melano/lysosomal compartments (Figure 5A). LysoTracker, which is largely independent of pH, stains the acidic compartments for size, number, and content of the acidic organelles, showed an increasing trend for ESO-NP-treated cells when compared to eNP-treated ones (Figure 5B). On the other hand, we observed an impact of ESO-NPs on the melanin content (Figure 5C). The declining profile of melanin levels for ESO-NP-treated cells (501 mel of 26.19%, LM56 of 4.85%, and LM38 of 17.65%) may be explained by the acknowledged inhibitory effect of ESO and other PPIs on tyrosinase activity.[47] Tyrosinase is a pH-dependent enzyme that catalyzes the conversion of tyrosine into dihydroxyphenylalanine (DOPA) and is located in stage II–IV melanosomes, which are lysosome-related organelles. Tyrosinase exerts its activity in a neutral/alkaline environment. Therefore, the blockade of V-ATPase, which keeps the lumen of melanosomes acidic, should result in melanin production. On the other hand, ESO can chelate copper and block the activity of this enzyme, leading to the opposite effect. We observed that compared to eNPs, ESO-NPs induced a reduction of melanin, even though this effect did not reach statistical significance. The decrease of intracellular acidity could represent a consequence of ESO mechanism of action, i.e., specific blockade of V-ATPase proton pumps located on lysosome-related organelles, including melanosomes, which are involved in the H^+ intake into the lysosomal lumen. As a prodrug, esomeprazole needs to be activated to exert its action. Our experiments suggest that the PPI activation takes place in the acidic environment of melanosomes once the NPs have efficiently delivered the drug. The effects induced by ESO-NPs did lead to a decreased intracellular acidity in comparison to eNPs, measured as decrease of LysoSensor levels.

This was repeatedly evident, but not statistically significant, for 501 mel and LM56 cells, whereas LM38 cells displayed similar LysoSensor levels regardless of NP content (Figure 5D, left panel). This may depend on the presence of melanosomes of different maturation stages in each cell.[48] Measurement of LysoTracker levels in the same samples showed an increase of gMFI that was statistically significant for 501 mel cells, suggesting that encapsulated ESO can impair the acidic compartments (Figure 5D, middle panel). Despite differences were modest, also the melanin content appeared to decrease in the presence of ESO-NPs in 501 mel and LM56 cells, whereas LM38 showed an opposite trend (Figure 5D, right panel). This result suggests that LM38 cells, which display higher intracellular acidity, differ in terms of ESO target expression, i.e., V-ATPase and tyrosinase. Finally, since extracellular acidity influences the expression of immune checkpoints such as PD-L1,[49] a target of immunotherapy with immune checkpoint inhibitors, we evaluated the

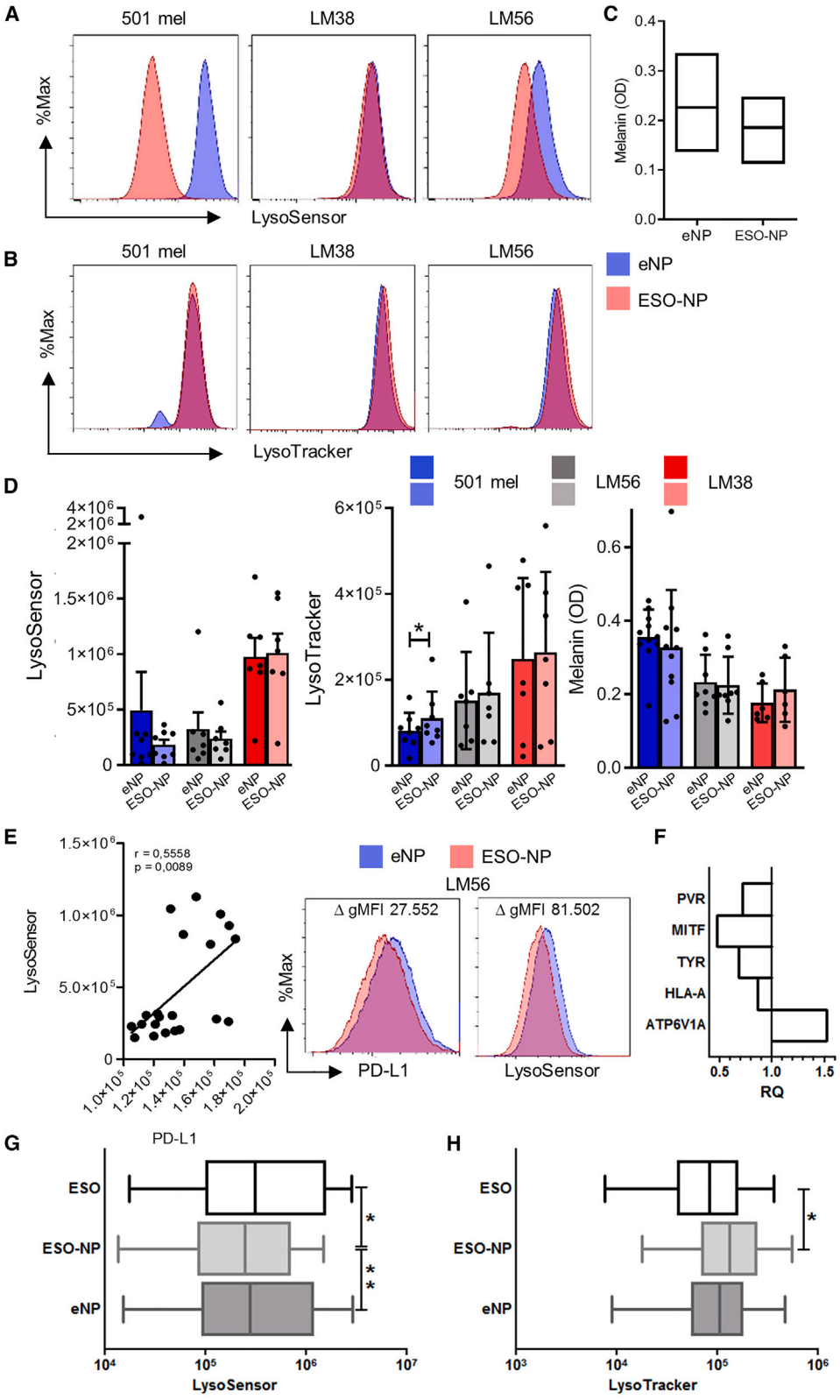

(legend on next page)

impact of ESO-NPs and eNPs on intracellular acidity within the context of surface PD-L1 expression. Our experiments showed that lysosomal/melanosomal acidity, measured as increasing LysoSensor gMFI, correlated positively with PD-L1 expression, suggesting that ESO-NP-induced alterations of lysosomal/melanosomal activity could impact the expression of this immune checkpoint (Figure 5E). Similarly, RNA analysis of ESO-NP-exposed 501 mel cells revealed a statistically significant downregulation of the immune checkpoint PVR/CD155 (28.1%), MITF (52.04%), and TYR (31.82%) and a slight but significant decrease of HLA-A expression (13.9%). In contrast, the VATPase subunit ATP6V1A displayed an upregulation of 51.87% (Figure 5F). These results further support the release and activity of ESO at melanosomal level, as documented by the impact on MITF, TYR, and ATP6V1A expression, whereas the decrease of PD-L1 and CD155 suggests that intracellular delivery of ESO via NPs contributes to a reduction of regulatory immune checkpoints involved in resistance to immune checkpoint blockade (ICB).[50] We also evaluated the effects of ESO-NPs in parallel with ESO solution that was applied at the same concentration as the one contained in the ESO-NPs. Under these conditions we could not detect a decrease of intracellular acidity, as was evident for ESO-NPs (Figure 5G). Similarly, increased LysoTracker values were assessable only in the presence of ESO-NPs, but not with soluble ESO (Figure 5H). Recorded effects were not related to cytotoxic effects of eNP or ESO-NPs, as the percentage of cells in the «alive» and the «dead » gates remained constant for all experimental conditions tested (Figure S2).

The most common genetic abnormality in melanoma is represented by BRAF mutations, which occur in 40%–50% of melanoma patients. All the melanoma cell lines we investigated here, with the exception of 501 mel, displayed the V600E mutation, resulting in a constitutive BRAF activation that leads to tumor-cell-intrinsic-driven increase of proliferation, invasion, and metastasis. BRAF mutation can also impact melanoma cell PD-L1 expression. Furthermore, the constitutive BRAF activation leads to TME modulations characterized by an increase of immune cells sustaining immune suppressive circuits, such as MDSCs, and a reduction of activated interferon gamma (IFNγ)-producing tumor infiltrating lymphocytes (TILs), with a consequently worse immunotherapy outcome. However, production of IFNγ during anti-tumor immune responses also induces PD-L1 expression in melanoma cells.[51] With this premise and given the potentially opposing effects of IFNγ in the TME,[52] we tested the activity of ESO-NPs on LM47 melanoma cells in the presence of IFNγ, which we added for the last 24 h of the 72-h culture period, to determine the impact of this pleiotropic cytokine on melanoma intracellular acidity in terms of LysoSensor and LysoTracker and PD-L1 expression. Results showed that PDL-1 was upregulated in the control condition (treated with empty NPs, eNPs) after culture with IFNγ as compared with eNPs in the absence of IFNγ. Of note, the presence of ESO-NPs reduced the expression of this immune checkpoint remarkably, also in the presence of IFNγ. As for the other melanoma cell lines, ESO-NPs induced a decrease of LysoSensor and minimally impacted LysoTracker, which was evident in LM47 cells both in the presence and absence of IFNγ (Figure 6A). Similarly, the decrease of PD-L1 and LysoSensor mediated by ESO-NPs was also stronger compared to soluble ESO both in the absence and presence of IFNγ, whereas LysoTracker values showed an opposite trend. In fact, LysoTracker gMFI levels were increased in the presence of ESO-NPs with respect to ESO free drug (Figure 6B), an effect that could be related to internalization of encapsulated versus free ESO as observed before (Figure 5G). Additionally, cell-cycle analysis showed that ESO-NPs induce an increase in G0/G1 cell-cycle arrest as compared to eNPs and ESO free drug (Figure S3). These results further corroborate our findings (Figures 3, 4, and 5) and demonstrate that ESO-NPs show activity under different conditions commonly prevailing the TME, such as secretion of IFNγ.

Effect of esomeprazole-loaded PLGA NPs on immunosuppressive myeloid cells

In the TME, the anti-tumor responses can be further limited by immune cells fostering immune suppression, such as T regulatory cells and MDSCs, which leads to the generation of resistance against cancer therapies, including ICI immunotherapy.[53] Given the strong endocytic and immune suppressive activities of monocytic MDSCs, a myeloid cell population that has been a long-standing focus of our research both *ex vivo* and *in vitro*,[54,55] we sought to investigate the activity of ESO-NPs on the myeloid immune suppressive phenotype of *in vitro* generated MDSCs and of MDSCs obtained from melanoma patients. To this aim, we induced MDSC phenotype in monocytes isolated from peripheral blood mononuclear cell (PBMC) of healthy donors (HDs, $n = 3$) with a cytokine cocktail containing granulocyte-macrophage colony-stimulating factor (GM-CSF), interleukin-6 (IL-6), and transforming growth factor β (TGF-β) for 72 h and then evaluated the effects of ESO-NP with respect to eNP after 24 h (Figures 7A–7D). Results show a decrease in the percentage of $CD14^+$ cells displaying a low or negative HLA-DR expression, the principal hallmark of monocytic MDSCs, which was evident

Figure 5. Effect of esomeprazole-encapsulated PLGA NPs on melanoma cells

(A–C) NPs containing esomeprazole (ESO-NP) or not (eNP) were incubated with melanoma cell lines for 72 h. Flow cytometry detection of (A) LysoSensor and (B) LysoTracker. (C) Melanin content was measured as optical densities (OD) by spectrophotometry.

(D) Summary of experiments showing LysoSensor, LysoTracker, and melanin content in the melanoma cell lines 501 mel, LM56, and LM38 incubated with eNP vs. ESO-NP. Statistically significant differences were recorded using paired t test: $*p \leq 0.05$.

(E) Spearman correlation analysis of PD-L1 surface expression measured by flow cytometry on melanoma cell lines and intracellular acidity measured via LysoSensor. Representative image of LM56 cells incubated with ESO-NP vs. eNPs for 72 h and evaluated for PD-L1 surface expression and intracellular acidity (LysoSensor) measured by flow cytometry.

(F) The RQ expression levels of selected genes in ESO-NP treated compared with eNP-treated 501 mel cells measured by qPCR. Significant differences are shown; $p \leq 0.01$, paired Student's t test.

(G and H) Effects of ESO-NP compared to ESO free drug on melanoma cell lines ($n = 3$); pooled results are shown. Data are represented as mean ± SD. Statistical significance was achieved with Friedman test and Dunn's multiple comparison. LysoSensor, $p = 0.0023$ (G); LysoTracker, $p = 0.0232$ (H). $*p \leq 0.05$; $**p \leq 0.01$.

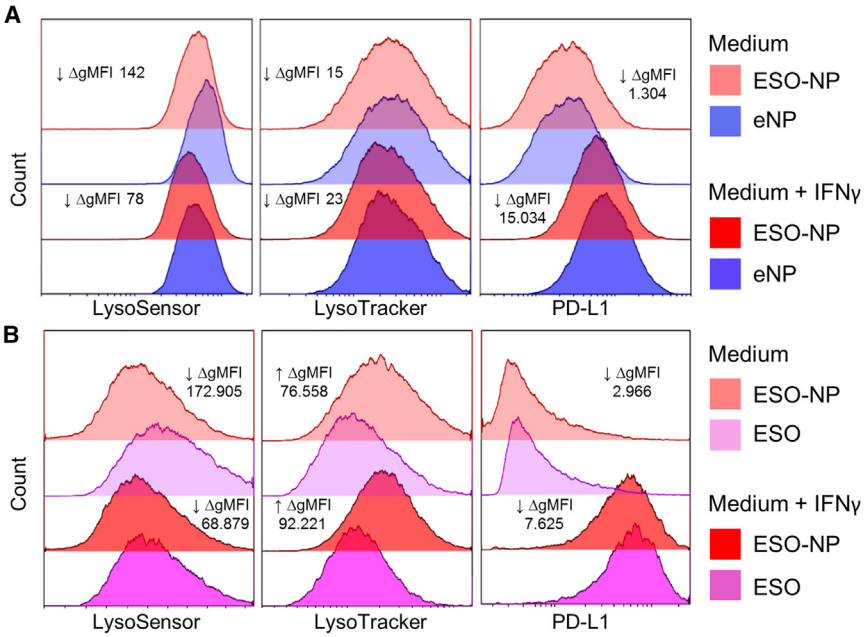

Figure 6. Effect of esomeprazole-encapsulated PLGA NPs on melanoma cells in TME-mimicking conditions

(A) NPs containing esomeprazole (ESO-NP) or not (eNP) were incubated with melanoma cell line LM47 for 72 h in the absence or presence of IFNγ (25 ng/mL). Flow cytometry detection of LysoSensor, LysoTracker, and PD-L1. The ΔgMFI values indicate the difference in gMFI as decrease in acidity in the melano/lysosomal compartment (LysoSensor and LysoTracker) and decrease of PD-L1 expression in ESO-NP conditions with respect to eNP.

(B) NPs containing esomeprazole (ESO-NP) or the ESO free drug at the same concentration as encapsulated ESO was incubated with melanoma cell line LM47 for 72 h in the absence or presence of IFNγ (25 ng/mL). Flow cytometry detection of LysoSensor, LysoTracker, and PD-L1. The ΔgMFI values indicate the difference in gMFI as decrease in intracellular acidity (LysoSensor), increase of the melano/lysosomal compartment (LysoTracker), and decrease of PD-L1 expression in ESO-NP conditions with respect to ESO.

for all HD-derived MDSCs incubated with ESO-NPs (Figure 7A). This reactivation in terms of HLA-DR upregulation observed in the presence of ESO-NPs was accompanied by an increase of CD86 co-stimulatory molecule expression and higher percentage of $CD14^+$ cells co-expressing HLA-DR and CD86 (Figure 7B). Similarly, ESO-NPs increased the percentage of $CD14^+$HLA-$DR^+CX3CR1^+$, a population of activated monocytes prone to extravasation and migration to TME (Figure 7C). No relevant modulation could be recorded for PD-L1, CD163, and CD206; these latter are associated with tolerance and immune suppression (Figure 7D). Interestingly, upon incubation of monocytes derived from peripheral blood of melanoma patients, we could instead observe a downregulation of PD-L1 after 24 h incubation with ESO-NPs, as compared to eNPs, which encompassed samples from all three patients. This was accompanied by a strong decrease of CD206 (Figure 7E). Patients' monocytes also displayed a downregulation of CD163 in the presence of ESO-NP with a concomitant increased expression of CD80 co-stimulatory molecule, as illustrated by the increase in percentage of $CD14^+CD163^-CD80^+$ (Figure 7F). Finally, the decreased production of cytokines associated with immune suppression by ESO-NP-treated monocytes, including IL-8, IL-6, and CCL2, confirmed the reprogramming of MDSCs at functional level (Figure 7G).

In summary, our results suggest that ESO-NPs can reach the melanosomal/lysosomal compartments of melanoma cells and release ESO with a consequent decrease of acidity and melanin content, potentially by inhibiting tyrosinase activity. This disruption of the endolysosomal compartment in cancer cells associated with pH alterations could contribute to avoid autophagy and consequent cancer progression and tumor immune escape.[56] Additionally, we observed that intracellular interventions targeting the acidity of endo-lysosomal compartment via NPs can impact the expression of proteins, such as the immune checkpoint PD-L1, highlighting the unique benefits of NP-assisted delivery of ESO. Immune cell studies confirmed the potential of ESO-NPs in reprogramming immunosuppressive myeloid cells, further highlighting the inhibitory activity on PD-L1 expression of encapsulated ESO in patient-derived MDSCs. Reversion of phenotype and functional traits associated with immune suppression induced by ESO-NPs corroborate the utility of NP-assisted delivery of ESO also in the immune cell setting.

Limitations of the study

In this study, we have shown that intracellular pH reprogramming of melanoma cells and MDSCs by ESO-NPs can potentially improve the response to immunotherapies as suggested by the altered expression level of proteins involved in resistance to cancer therapy and immune suppression. The major limitation of the study is the lack of *in vivo* studies, which are needed to confirm not only the immune responses but also the biodistribution profile of the ESO-NPs.

RESOURCE AVAILABILITY

Lead contact

Requests for further information and resources should be directed to and will be fulfilled by the lead contact, Veronica Huber (veronica.huber@istitutotumori.mi.it).

Materials availability

This study did not generate new unique reagents or cell lines.

Data and code availability

- Data reported in this paper will be shared by the lead contact upon request.
- This paper does not report original code.
- Any additional information about the data reported in this paper will be shared by the lead contact upon request.

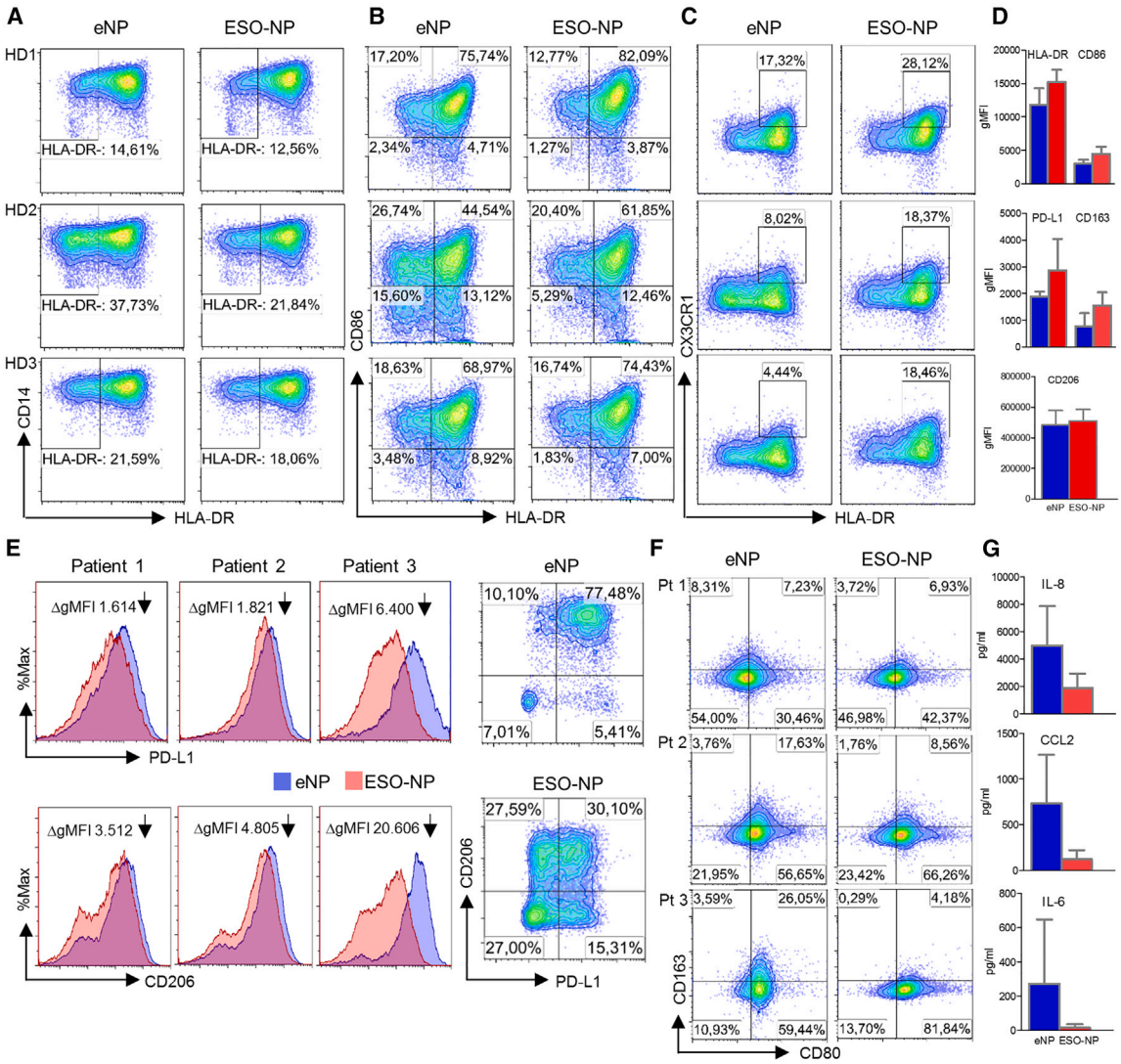

Figure 7. Effect of esomeprazole-loaded PLGA NPs on myeloid-derived suppressor cells (MDSCs) to revert immunosuppressive features

(A–D) NPs containing esomeprazole (ESO-NP) or not (eNP) were incubated with MDSCs generated *in vitro* from isolated healthy donors' (HD, $n = 3$) monocytes with cytokines (GM-CSF, IL-6, TGF-β), for 72 h, prior to incubation with ESO-NP or eNP for further 24 h. (A) Decrease of the % of $CD14^{+}HLA\text{-}DR^{neg}$ myeloid cells, associated with cancer immune suppression, in the presence of ESO-NP with respect to eNP. (B) Increase of % functional monocytes expressing CD86 co-stimulatory molecule and HLA-DR in the presence of ESO-NP with respect to eNP. (C) Increase of % activated monocytes expressing HLA-DR and CX3CR1 prone to extravasation and migration to TME. (D) Bar charts summarizing changes in expression (gMFI) of markers detected by flow cytometry on *in vitro*-generated MDSCs from HD monocytes conditioned with ESO-NP and eNP.

(E–G) NPs containing esomeprazole (ESO-NP) or not (eNP) were incubated for 24 h with monocytes isolated from PBMC of melanoma patients ($n = 3$) and presenting typical MDSC alterations. (E) Decrease of expression of PD-L1 and CD206 immune-suppression-associated markers in the presence of ESO-NP with respect to eNP. Histograms show gMFI of PD-L1 and CD206; dot plots show a representative example (patient 3) of the increase of PD-L1 and CD206 double-negative cells in the presence of ESO-NP. (F) Loss of immune-suppression-associated marker CD163 and gain of co-stimulatory molecule CD80 expression (single positive for CD80) by melanoma patients' (Pt 1–3) derived monocytes in the presence of ESO-NP with respect to eNP. (G) Decreased release of cytokines associated with immune suppression and tumor promotion (IL-8, CCL2, IL-6) by melanoma-patients-derived myeloid cells incubated with ESO-NP, as compared to eNP. HD, healthy donor; Pt, patient.

ACKNOWLEDGMENTS

We thank Simona Frigerio and Paola Squarcina for technical assistance. This research was funded by EU grant PRECIOUS (686089) and supported by AIRC IG-25078 grant (V.H.). C.F. received the NWO Spinoza grant, ERC Advanced Grant Pathfinder (269019), and Dutch cancer society award 2009-4402. Graphical abstract was created with BioRender.com.

AUTHOR CONTRIBUTIONS

Conceptualization, L.R., C.G.F., V.H., and O.T.; investigation, N.C., W.B., A.M., J.S., A.C., G.L., and E.D'A.; writing—original draft, N.C., W.B., A.M., V.H., and O.T.; writing—review and editing, N.C., W.B., A.M., J.S., A.C., G.L., E.D'A., and E.N.; funding acquisition, L.R., C.G.F., and V.H.; visualization, V.H. and O.T; supervision, V.H. and O.T.

DECLARATION OF INTERESTS

The authors declare no competing interests.

STAR★METHODS

Detailed methods are provided in the online version of this paper and include the following:

- KEY RESOURCES TABLE
- EXPERIMENTAL MODEL AND STUDY PARTICIPANT DETAILS
  - Cell lines
  - Human PBMC samples
- METHOD DETAILS
  - Materials
  - Preparation of PLGA nanoparticles
  - Preparation of PLGA core-shell nanoparticles
  - Characterization of PLGA nanoparticles
  - *In vitro* studies
- QUANTIFICATION AND STATISTICAL ANALYSIS

SUPPLEMENTAL INFORMATION

Supplemental information can be found online at https://doi.org/10.1016/j.isci.2024.111559.

Received: March 14, 2024
Revised: August 4, 2024
Accepted: December 5, 2024
Published: December 9, 2024

REFERENCES

1. Estrella, V., Chen, T., Lloyd, M., Wojtkowiak, J., Cornnell, H.H., Ibrahim-Hashim, A., Bailey, K., Balagurunathan, Y., Rothberg, J.M., Sloane, B.F., et al. (2013). Acidity generated by the tumor microenvironment drives local invasion. Cancer Res. *73*, 1524–1535. https://doi.org/10.1158/0008-5472.CAN-12-2796.
2. Yang, O.C.Y., and Loh, S.H. (2019). Acidic stress triggers sodium-coupled bicarbonate transport and promotes survival in A375 human melanoma cells. Sci. Rep. *9*, 6858. https://doi.org/10.1038/s41598-019-43262-y.
3. Koirala, M., Shashikala, H.B.M., Jeffries, J., Wu, B., Loftus, S.K., Zippin, J.H., and Alexov, E. (2021). Computational investigation of the pH dependence of stability of melanosome proteins: implication for melanosome formation and disease. Int. J. Mol. Sci. *22*, 8273. https://doi.org/10.3390/ijms22158273.
4. Ambrosio, A.L., Boyle, J.A., Aradi, A.E., Christian, K.A., and Di Pietro, S.M. (2016). TPC2 controls pigmentation by regulating melanosome pH and size. Proc. Natl. Acad. Sci. USA *113*, 5622–5627. https://doi.org/10.1073/pnas.1600108113.
5. Matsui, M.S., Petris, M.J., Niki, Y., Karaman-Jurukovska, N., Muizzuddin, N., Ichihashi, M., and Yarosh, D.B. (2015). Omeprazole, a gastric proton pump inhibitor, inhibits melanogenesis by blocking ATP7A trafficking. J. Invest. Dermatol. *135*, 834–841. https://doi.org/10.1038/jid.2014.461.
6. Baek, S.H., and Lee, S.H. (2016). Omeprazole inhibits melanin biosynthesis in melan-a cells and zebrafish. Exp. Dermatol. *25*, 239–241. https://doi.org/10.1111/exd.12915.
7. Parks, S.K., Mueller-Klieser, W., and Pouysségur, J. (2020). Lactate and acidity in the cancer microenvironment. Annu. Rev. Cell Biol. *4*, 141–158. https://doi.org/10.1146/annurev-cancerbio-030419-033556.
8. Walsh, M., Fais, S., Spugnini, E.P., Harguindey, S., Abu Izneid, T., Scacco, L., Williams, P., Allegrucci, C., Rauch, C., and Omran, Z. (2015). Proton pump inhibitors for the treatment of cancer in companion animals. J. Exp. Clin. Cancer Res. *34*, 93. https://doi.org/10.1186/s13046-015-0204-z.
9. Bellone, M., Calcinotto, A., Filipazzi, P., De Milito, A., Fais, S., and Rivoltini, L. (2013). The acidity of the tumor microenvironment is a mechanism of immune escape that can be overcome by proton pump inhibitors. Oncolmmunology *2*, e22058. https://doi.org/10.4161/onci.22058.
10. Wang, Y., Ding, Y., Deng, Y., Zheng, Y., and Wang, S. (2020). Role of myeloid-derived suppressor cells in the promotion and immunotherapy of colitis-associated cancer. J. Immunother. Cancer *8*, e000609. https://doi.org/10.1136/jitc-2020-000609.
11. Zhu, J., Fan, J., Xia, Y., Wang, H., Li, Y., Feng, Z., and Fu, C. (2023). Potential targets and applications of nanodrug targeting myeloid cells in osteosarcoma for the enhancement of immunotherapy. Front. Pharmacol. *14*, 1271321. https://doi.org/10.3389/fphar.2023.1271321.
12. Pérez-Herrero, E., and Fernández-Medarde, A. (2021). The reversed intra- and extracellular pH in tumors as a unified strategy to chemotherapeutic delivery using targeted nanocarriers. Acta Pharm. Sin. B *11*, 2243–2264. https://doi.org/10.1016/j.apsb.2021.01.012.
13. Huber, V., Camisaschi, C., Berzi, A., Ferro, S., Lugini, L., Triulzi, T., Tuccitto, A., Tagliabue, E., Castelli, C., and Rivoltini, L. (2017). Cancer acidity: An ultimate frontier of tumor immune escape and a novel target of immunomodulation. Semin. Cancer Biol. *43*, 74–89. https://doi.org/10.1016/j.semcancer.2017.03.001.
14. Luciani, F., Spada, M., De Milito, A., Molinari, A., Rivoltini, L., Montinaro, A., Marra, M., Lugini, L., Logozzi, M., Lozupone, F., et al. (2004). Effect of proton pump inhibitor pretreatment on resistance of solid tumors to cytotoxic drugs. J. Natl. Cancer Inst. *96*, 1702–1713. https://doi.org/10.1093/jnci/djh305.
15. Wang, B.Y., Zhang, J., Wang, J.L., Sun, S., Wang, Z.H., Wang, L.P., Zhang, Q.L., Lv, F.F., Cao, E.Y., Shao, Z.M., et al. (2015). Intermittent high dose proton pump inhibitor enhances the antitumor effects of chemotherapy in metastatic breast cancer. J. Exp. Clin. Cancer Res. *34*, 85. https://doi.org/10.1186/s13046-015-0194-x.
16. Homicsko, K., Dummer, R., Hoeller, C., Wolchok, J.D., Hodi, F.S., Larkin, J., Ascierto, P.A., Atkinson, V., Robert, C., Postow, M.A., et al. (2022). Proton pump inhibitor use and efficacy of Nivolumab and Ipilimumab in advanced melanoma. Cancers *14*, 2300. https://doi.org/10.3390/cancers14092300.
17. Lee, T., Kim, K.S., and Na, K. (2022). Intracellular pH-regulating nanoparticles to improve anticancer drug efficacy for cancer treatment. Biomacromolecules *23*, 4786–4794. https://doi.org/10.1021/acs.biomac.2c00952.
18. Belhadj, Z., He, B., Fu, J., Zhang, H., Wang, X., Dai, W., and Zhang, Q. (2020). Regulating interactions between targeted nanocarriers and mononuclear phagocyte system via an esomeprazole-based preconditioning strategy. Int. J. Nanomed. *15*, 6385–6399. https://doi.org/10.2147/IJN.S258054.
19. Lasser, S.A., Ozbay Kurt, F.G., Arkhypov, I., Utikal, J., and Umansky, V. (2024). Myeloid-derived suppressor cells in cancer and cancer therapy. Nat. Rev. Clin. Oncol. *21*, 147–164. https://doi.org/10.1038/s41571-023-00846-y.
20. Rennick, J.J., Johnston, A.P.R., and Parton, R.G. (2021). Key principles and methods for studying the endocytosis of biological and nanoparticle therapeutics. Nat. Nanotechnol. *16*, 266–276. https://doi.org/10.1038/s41565-021-00858-8.
21. Operti, M.C., Fecher, D., van Dinther, E.A.W., Grimm, S., Jaber, R., Figdor, C.G., and Tagit, O. (2018). A comparative assessment of continuous production techniques to generate sub-micron size PLGA particles. Int. J. Pharm. *550*, 140–148. https://doi.org/10.1016/j.ijpharm.2018.08.044.
22. Operti, M.C., Dölen, Y., Keulen, J., van Dinther, E.A.W., Figdor, C.G., and Tagit, O. (2019). Microfluidics-assisted size tuning and biological evaluation of PLGA particles. Pharmaceutics *11*, 590. https://doi.org/10.3390/pharmaceutics11110590.
23. Operti, M.C., Bernhardt, A., Grimm, S., Engel, A., Figdor, C.G., and Tagit, O. (2021). PLGA-based nanomedicines manufacturing: Technologies

overview and challenges in industrial scale-up. Int. J. Pharm. *605*, 120807. https://doi.org/10.1016/j.ijpharm.2021.120807.

24. Operti, M.C., Bernhardt, A., Pots, J., Sincari, V., Jager, E., Grimm, S., Engel, A., Benedikt, A., Hrubý, M., De Vries, I.J.M., et al. (2022). Translating the manufacture of immunotherapeutic PLGA nanoparticles from lab to industrial scale: process transfer and *in vitro* testing. Pharmaceutics *14*, 1690. https://doi.org/10.3390/pharmaceutics14081690.
25. Swider, E., Maharjan, S., Houkes, K., van Riessen, N.K., Figdor, C., Srinivas, M., and Tagit, O. (2019). Förster resonance energy transfer-based stability assessment of PLGA nanoparticles *in vitro* and *in vivo*. ACS Appl. Bio Mater. *2*, 1131–1140. https://doi.org/10.1021/acsabm.8b00754.
26. Dölen, Y., Valente, M., Tagit, O., Jäger, E., Van Dinther, E.A.W., van Riessen, N.K., Hruby, M., Gileadi, U., Cerundolo, V., and Figdor, C.G. (2020). Nanovaccine administration route is critical to obtain pertinent iNKt cell help for robust anti-tumor T and B cell responses. OncoImmunology *9*, 1738813. https://doi.org/10.1080/2162402X.2020.1738813.
27. Alai, M., and Lin, W.J. (2014). Novel lansoprazole-loaded nanoparticles for the treatment of gastric acid secretion-related ulcers: *in vitro* and *in vivo* pharmacokinetic pharmacodynamic evaluation. AAPS J. *16*, 361–372. https://doi.org/10.1208/s12248-014-9564-0.
28. Bhattacharya, S., Khanam, J., Sarkar, P., and Pal, T.K. (2018). A chemotherapeutic approach targeting the acidic tumor microenvironment: combination of a proton pump inhibitor and paclitaxel for statistically optimized nanotherapeutics. RSC Adv. *9*, 240–254. https://doi.org/10.1039/c8ra08924h.
29. Gralnek, I.M., Dulai, G.S., Fennerty, M.B., and Spiegel, B.M.R. (2006). Esomeprazole versus other proton pump inhibitors in erosive esophagitis: a meta-analysis of randomized clinical trials. Clin. Gastroenterol. Hepatol. *4*, 1452–1458. https://doi.org/10.1016/j.cgh.2006.09.013.
30. Castell, D.O., Kahrilas, P.J., Richter, J.E., Vakil, N.B., Johnson, D.A., Zuckerman, S., Skammer, W., and Levine, J.G. (2002). Esomeprazole (40 mg) compared with lansoprazole (30 mg) in the treatment of erosive esophagitis. Am. J. Gastroenterol. *97*, 575–583. https://doi.org/10.1111/j.1572-0241.2002.05532.x.
31. Stipa, P., Marano, S., Galeazzi, R., Minnelli, C., Mobbili, G., and Laudadio, E. (2021). Prediction of drug-carrier interactions of PLA and PLGA drug-loaded nanoparticles by molecular dynamics simulations. Eur. Polym. J. *147*, 110292. https://doi.org/10.1016/j.eurpolymj.2021.110292.
32. Hua, Y., Su, Y., Zhang, H., Liu, N., Wang, Z., Gao, X., Gao, J., and Zheng, A. (2021). Poly(lactic-co-glycolic acid) microsphere production based on quality by design: a review. Drug Deliv. *28*, 1342–1355. https://doi.org/10.1080/10717544.2021.1943056.
33. Hoda, M., Sufi, S.A., Cavuturu, B., and Rajagopalan, R. (2018). Stabilizers influence drug-polymer interactions and physicochemical properties of disulfiram-loaded poly-lactide-co-glycolide nanoparticles. Future Sci. OA *4*, FSO263. https://doi.org/10.4155/fsoa-2017-0091.
34. Staal, A.H.J., Becker, K., Tagit, O., Koen van Riessen, N., Koshkina, O., Veltien, A., Bouvain, P., Cortenbach, K.R.G., Scheenen, T., Flögel, U., et al. (2020). In vivo clearance of ^{19}F MRI imaging nanocarriers is strongly influenced by nanoparticle ultrastructure. Biomaterials *261*, 120307. https://doi.org/10.1016/j.biomaterials.2020.120307.
35. Rivoltini, L., Barracchini, K.C., Viggiano, V., Kawakami, Y., Smith, A., Mixon, A., Restifo, N.P., Topalian, S.L., Simonis, T.B., and Rosenberg, S.A. (1995). Quantitative correlation between HLA class I allele expression and recognition of melanoma cells by antigen-specific cytotoxic T lymphocytes. Cancer Res. *55*, 3149–3157.
36. Daniotti, M., Oggionni, M., Ranzani, T., Vallacchi, V., Campi, V., Di Stasi, D., Torre, G.D., Perrone, F., Luoni, C., Suardi, S., et al. (2004). BRAF alterations are associated with complex mutational profiles in malignant melanoma. Oncogene *23*, 5968–5977. https://doi.org/10.1038/sj.onc.1207780.
37. Vergani, E., Vallacchi, V., Frigerio, S., Deho, P., Mondellini, P., Perego, P., Cassinelli, G., Lanzi, C., Testi, M.A., Rivoltini, L., et al. (2011). Identification of MET and SRC activation in melanoma cell lines showing primary resistance to PLX4032. Neoplasia *13*, 1132–1142. https://doi.org/10.1593/neo.111102.
38. Sachs, G., Shin, J.M., and Howden, C.W. (2006). Review article: the clinical pharmacology of proton pump inhibitors. Aliment. Pharmacol. Ther. *23*, 2–8. https://doi.org/10.1111/j.1365-2036.2006.02943.x.
39. van Hunsel, F., de Jong, L., and de Vries, T. (2016). (Es)omeprazole and discoloration of regurgitated gastric contents in infants: worrying for care-takers and a sign of a reduced bioavailability. J. Pediatr. Pharmacol. Therapeut. *21*, 260–262. https://doi.org/10.5863/1551-6776-21.3.260.
40. Gul, W., Sajid, S., Hamid, F., Bhatti, S., and Prof, A. (2015). Effect of acidic Ph. and heat on the degradation of omeprazole and Esomeprazole. Pharm. Innov. *4*, 19–21. www.drugbank.ca/drug/db00338.
41. Riedel, A., and Leopold, C.S. (2005). Quantification of omeprazole degradation by enteric coating polymers: an UV-VIS spectroscopy study. Pharmazie *60*, 126–130.
42. Ayub, A., and Wettig, S. (2022). An overview of nanotechnologies for drug delivery to the brain. Pharmaceutics *14*, 224. https://doi.org/10.3390/pharmaceutics14020224.
43. Jójárt, B., Poša, M., Fiser, B., Szőri, M., Farkaš, Z., and Viskolcz, B. (2014). Mixed micelles of sodium cholate and sodium dodecylsulphate 1:1 binary mixture at different temperatures–experimental and theoretical investigations. PLoS One *9*, e102114. https://doi.org/10.1371/journal.pone.0102114.
44. Khemani, M., Sharon, M., and Sharon, M. (2012). Encapsulation of berberine in nano-sized PLGA synthesized by emulsification method. Int. Sch. Res. Netw. ISRN Nanotechnol. *2012*, 187354. https://doi.org/10.5402/2012/187354.
45. Panyam, J., Dali, M.M., Sahoo, S.K., Ma, W., Chakravarthi, S.S., Amidon, G.L., Levy, R.J., and Labhasetwar, V. (2003). Polymer degradation and *in vitro* release of a model protein from poly(D,L-lactide-co-glycolide) nano- and microparticles. J. Contr. Release *92*, 173–187. https://doi.org/10.1016/s0168-3659(03)00328-6.
46. Zeng, J., Martin, A., Han, X., Shirihai, O.S., and Grinstaff, M.W. (2019). Biodegradable PLGA nanoparticles restore lysosomal acidity and protect neural PC-12 cells against mitochondrial toxicity. Ind. Eng. Chem. Res. *58*, 13910–13917. https://doi.org/10.1021/acs.iecr.9b02003.
47. Baek, S.H., and Lee, S.H. (2015). Proton pump inhibitors decrease melanogenesis in melanocytes. Biomed. Rep. *3*, 726–730. https://doi.org/10.3892/br.2015.492.
48. Wakamatsu, K., Zippin, J.H., and Ito, S. (2021). Chemical and biochemical control of skin pigmentation with special emphasis on mixed melanogenesis. Pigment Cell Melanoma Res. *34*, 730–747. https://doi.org/10.1111/pcmr.12970.
49. Mori, D., Tsujikawa, T., Sugiyama, Y., Kotani, S.I., Fuse, S., Ohmura, G., Arai, A., Kawaguchi, T., Hirano, S., Mazda, O., and Kishida, T. (2021). Extracellular acidity in tumor tissue upregulates programmed cell death ligand 1 expression on tumor cells via proton-sensing G protein-coupled receptors. Int. J. Cancer *149*, 2116–2124. https://doi.org/10.1002/ijc.33786.
50. Lepletier, A., Madore, J., O'Donnell, J.S., Johnston, R.L., Li, X.Y., McDonald, E., Ahern, E., Kuchel, A., Eastgate, M., Pearson, S.A., et al. (2020). Tumor CD155 expression is associated with resistance to anti-PD1 immunotherapy in metastatic melanoma. Clin. Cancer Res. *26*, 3671–3681. https://doi.org/10.1158/1078-0432.CCR-19-3925.
51. Górniak, P., Wasylecka-Juszczyńska, M., Ługowska, I., Rutkowski, P., Polak, A., Szydłowski, M., and Juszczyński, P. (2020). BRAF inhibition curtails IFN-gamma-inducible PD-L1 expression and upregulates the immunoregulatory protein galectin-1 in melanoma cells. Mol. Oncol. *14*, 1817–1832. https://doi.org/10.1002/1878-0261.12695.
52. Gocher, A.M., Workman, C.J., and Vignali, D.A.A. (2022). Interferon-γ: teammate or opponent in the tumour microenvironment? Nat. Rev. Immunol. *22*, 158–172. https://doi.org/10.1038/s41577-021-00566-3.
53. Fares, C.M., Van Allen, E.M., Drake, C.G., Allison, J.P., and Hu-Lieskovan, S. (2019). Mechanisms of resistance to immune checkpoint blockade: why

does checkpoint inhibitor immunotherapy not work for all patients? Am. Soc. Clin. Oncol. Educ. Book. *39*, 147–164. https://doi.org/10.1200/EDBK_240837.

54. Filipazzi, P., Valenti, R., Huber, V., Pilla, L., Canese, P., Iero, M., Castelli, C., Mariani, L., Parmiani, G., and Rivoltini, L. (2007). Identification of a new subset of myeloid suppressor cells in peripheral blood of melanoma patients with modulation by a granulocyte-macrophage colony-stimulation factor-based antitumor vaccine. J. Clin. Oncol. *25*, 2546–2553. https://doi.org/10.1200/JCO.2006.08.5829.

55. Huber, V., Vallacchi, V., Fleming, V., Hu, X., Cova, A., Dugo, M., Shahaj, E., Sulsenti, R., Vergani, E., Filipazzi, P., et al. (2018). Tumor-derived microRNAs induce myeloid suppressor cells and predict immunotherapy resistance in melanoma. J. Clin. Invest. *128*, 5505–5516. https://doi.org/10.1172/JCI98060.

56. Bestion, E., Raymond, E., Mezouar, S., and Halfon, P. (2023). Update on autophagy inhibitors in cancer: opening up to a therapeutic combination with immune checkpoint inhibitors. Cells *12*, 1702. https://doi.org/10.3390/cells12131702.

STAR★METHODS

KEY RESOURCES TABLE

REAGENT or RESOURCE	SOURCE	IDENTIFIER
Antibodies		
PE-CF594 Mouse Anti-Human CD274 (clone MIH1)	BD Biosciences	Cat Nr. 563742; RRID: AB_2738400
PC7 Mouse Anti-Human CD274 (clone PD-L1)	Beckman Coulter	Cat Nr. A78884
FITC Mouse anti-human CD206 (MMR) (Clone 15-2)	Biolegend	Cat Nr 321104; RRID: AB_571905
BD Pharmingen APC Mouse Anti-Human CD206 (Clone 19.2)	BD Biosciences	Cat Nr 550889; RRID: AB_398476
BD Pharmingen PE Mouse Anti-Human CD86 (Clone 2331 (FUN-1))	BD Biosciences	Cat Nr 555658; RRID: AB_396013
BD Pharmingen PerCP-Cy5.5 Mouse Anti-Human CD163 (Clone GHI/61)	BD Biosciences	Cat Nr 563887; RRID: AB_2738467
CD14-APC-Alexa Fluor 750 (Clone RMO52)	Beckman Coulter	Cat Nr B92421; RRID: AB_2909815
Anti-HLA-DR-APC (Clone Immu-357)	Beckman Coulter	Cat Nr IM3635; RRID: AB_130796
BD Pharmingen PE Mouse Anti-Human HLA-DR (Clone TU36)	BD Biosciences	Cat Nr 555561; RRID: AB_395943
BD Pharmingen FITC Mouse Anti-Human CD80 (Clone L307.4)	BD Biosciences	Cat Nr 560926; RRID: AB_396605
BD OptiBuild™ BV510 Rat Anti-Human CX3CR1 (Clone 2A9-1)	BD Biosciences	Cat Nr 744487; RRID: AB_2742267
FcR Blocking Reagent, human	Miltenyi Biotec	Cat Nr 130-059-901; RRID: AB_2892112
CD14 MicroBeads, human	Miltenyi Biotec	Cat Nr 130-050-201; RRID: AB_2665482
Biological samples		
Human peripheral blood monocytes	Healthy donors (INT61/20)	N/A
Human peripheral blood monocytes	Melanoma patients (INT27/14)	N/A
Chemicals, peptides, and recombinant proteins		
Recombinant Human GM-CSF	PeproTech	Cat Nr 300-03; GenPept: P04141
Recombinant Human IL-6	PeproTech	Cat Nr 200-06; GenPept: P05231
Human TGF-β1	PeproTech	Cat Nr 100-21-50UG
Recombinant Human IFN-γ	Thermo Fisher Scientific	Cat Nr 300-02; GenPept: P01579.1
Esomeprazole sodium	Abcam	Cat Nr ab120500 CAS Nr 161796-78-7
Poly(D,L-lactide-co-glycolide), PLGA	Evonik	Cat Nr 719897 CAS Nr 26780-50-7
Poly(vinyl alcohol)	Sigma-Aldrich	Cat Nr 360627 CAS Nr 9002-89-5
Atto 647N	Sigma-Aldrich	Cat Nr 04507 CAS Nr 906664-68-4
BODIPY-FL C12	Thermo Fisher Scientific	Cat Nr D3822 CAS Nr 158757-79-0
Propidium Iodide	eBioscience	BMS500FI/300
Critical commercial assays		
LysoSensor Green DND-189 - Special Packaging	Thermo Fisher Scientific	Cat Nr L7535
LysoTracker Red DND-99, special packaging	Thermo Fisher Scientific	Cat Nr L7528
BD™ Cytometric Bead Array (CBA) Human IL-8 Flex Set	BD Biosciences	Cat Nr 558277; RRID: AB_2869133; BP: A9
BD™ Cytometric Bead Array (CBA) Human MCP-1 Flex Set	BD Biosciences	Cat Nr 558287; RRID: AB_2869139; BP: D8

(*Continued on next page*)

Continued

REAGENT or RESOURCE	SOURCE	IDENTIFIER
BD™ Cytometric Bead Array (CBA) Human IL-6 Flex Set	BD Biosciences	Cat Nr 558276; RRID: AB_2869132; BP: A7
miRNeasy Mini Kit (50)	Qiagen	Cat Nr /; ID: 217004
High-Capacity cDNA Reverse Transcription Kit	Thermo Fisher Scientific	Cat Nr 4368814
TaqMan™ PreAmp Master Mix Kit	Thermo Fisher Scientific	Cat Nr 4384267
Gene Print 10 System	Promega	Cat Nr B9510
Experimental models: Cell lines		
501 mel	Surgery Branch, Clinical Oncology Program, National Cancer Institute, NIH, Bethesda, Maryland 20892, USA	Rivoltini et al. Ref.[35]
LM38, LM47, LM56	Fondazione IRCCS Istituto Nazionale Tumori (Milan, Italy)	Daniotti et al. https://doi.org/10.1038/sj.onc.1207780. Ref.[36]
Oligonucleotides		
TaqMan™ Gene Expression Assay ATP6V1A	Thermo Fisher Scientific	Cat Nr 4331182; ID: Hs01097169_m1
TaqMan™ Gene Expression Assay MITF	Thermo Fisher Scientific	Cat Nr 4331182; ID: Hs00165156_m1
TaqMan™ Gene Expression Assay HLA-A	Thermo Fisher Scientific	Cat Nr 4331182; ID: Hs01058806_g1
TaqMan™ Gene Expression Assay PVR/CD155	Thermo Fisher Scientific	Cat Nr 4331182; ID: Hs00197846_m1
TaqMan™ Gene Expression Assay TYR	Thermo Fisher Scientific	Cat Nr 4331182; ID: Hs00165976_m1
Software and algorithms		
Prism 5.0 and 8.0	GraphPad	N/A
Kaluza Analysis Software	Beckman Coulter	N/A
FCAP Array Software for Cytometric Bead Array (CBA)	BD	N/A
QuantStudio 7 Flex Real-Time PCR System Software	Thermo Fisher Scientific	N/A
Biorender	http://biorender.com	N/A

EXPERIMENTAL MODEL AND STUDY PARTICIPANT DETAILS

Cell lines

The melanoma cell lines included 501 mel[35] and LM38, LM47 and LM56, which were obtained at Fondazione IRCCS Istituto Nazionale Tumori (Milan, Italy) from patient tumor samples[36]; cells were cultured at 37°C and 5% CO_2 atmosphere in RPMI 1640 medium with 10% FBS, L-Glutamine, penicillin and streptomycin, were passaged twice a week according to their growth rate and periodically checked for mycoplasma and authentication by STR analysis (Gene Print 10 System, Promega).

Human PBMC samples

Peripheral blood samples were collected from healthy donors (n = 3; 3 males) and stage III melanoma patients (n = 3; 3 males) under INT61/20 and INT27/14 after approval by the Independent Ethics Committee of Fondazione IRCCS Istituto Nazionale dei Tumori, Milan, Italy. Subjects were between 20 and 55 years of age. All subjects provided written informed consent before sample collection.

METHOD DETAILS

Materials

Esomeprazole sodium (ab120500; lot: APN11069-1-1) was purchased from ABCAM. Poly-(D,L-lactic-co-glycolic acid), PLGA RESOMER® RG 502H with a 50:50 ratio of lactic acid: glycolic acid was obtained from Evonik Nutrition and Care GmbH. Polyvinyl alcohol (PVA, 9.000 –10.000 Mw, 80% hydrolysed) was purchased from Sigma-Aldrich.

Atto647N was from Sigma-Aldrich and BODIPY-FL C12 was from ThermoFisher Scientific. Dichloromethane (DCM ≥99 %), dimethyl sulfoxide (DMSO ≥99.9%), 1N hydrochloric acid (HCl), 2N sodium hydroxide (NaOH), sodium cholate and glacial acetic

acid were obtained from Merck. Borate buffer (pH 10 and 11) was prepared by using 0.05 M sodium tetraborate and 0.1M NaOH. Trifluoroacetic acid (TFA), trichloroacetic acid (TCA), 3-(4,5-dimethylthiazol-2-yl)- 2,5-diphenyltetrazolium bromide (MTT reagent), and 2-Mercaptoethanol (BME) were obtained from Sigma-Aldrich. 4-(Dimethylamino)benzaldehyde (DMAB) was purchased from Honeywell™ Fluka™ (Thermo Fisher Scientific). LysoTracker Red DND-99 and LysoSensor Green DND-189 were purchased from Invitrogen. Antibodies conjugated to different fluorochromes against human PD-L1 (CD274), CD206, CD163, CX3CR1, HLA-DR, CD80, CD86 were purchased from Beckman Coulter and Becton Dickinson. Recombinant cytokines (GM-CSF, IL-6, TGFβ and IFNγ) for *in vitro* cultures of melanoma and myeloid cells were purchased from Peprotech; CD14 isolation beads human and Fc blocking reagent were purchased from Miltenyi Biotec.

Preparation of PLGA nanoparticles

NPs encapsulating esomeprazole were prepared by probe sonication method. In brief, 500 μL of 20 mg/mL esomeprazole (dissolved in ultrapure water, PBS pH 7.4 or borate buffer pH 10 or 11) was added to a 1.5 mL of PLGA solution (33% in DCM) and emulsified for 10 – 15 sec at 20% amplitude (10 Watts) using a probe sonicator equipped with a 6.3 mm microtip (Branson Ultrasonics, St. Louis, USA). This primary emulsion was added to 12.5 mL of 2 % (w/v) PVA solution and was emulsified further for 2 min at 20% amplitude. When particles were prepared in different batch sizes, the volume ratio of ESO: PLGA: PVA was kept as 1: 3: 25. The organic solvent was evaporated by stirring overnight at 4°C. The particles were collected by centrifugation (21'300 × g, 35 min), washed thrice with ultrapure water, then lyophilized.

Preparation of PLGA core-shell nanoparticles

Core-shell NPs encapsulating ESO were prepared as described in.[34] In brief, 500 μL of 20 mg/mL esomeprazole dissolved borate buffer (pH 11) was added to 1.5 mL of PLGA solution (33% in DCM) and was mixed by vigorous pipetting. This mixture was added to 12.5 mL of 1.5% sodium cholate and emulsified for 2 min at 20% amplitude (10 Watts) using a probe sonicator equipped with a 6.3 mm microtip (Branson Ultrasonics, St. Louis, USA). The organic solvent was evaporated by stirring overnight at 4°C. Next, 7 g of 2 % (w/v) PVA solution was added, and the solution was stirred at 4°C for 3 to 5 days to exchange the sodium cholate with PVA. The particles were collected by centrifugation (21'300 × g, 35 min), washed thrice with ultrapure water, and then lyophilized for 48 hours.

Fluorescently labelled NPs were prepared following the described protocols with the addition of Atto647N (0.3 w/w %) or BODIPY-FL C12 (1.0 w/w %) to the organic phase.

Characterization of PLGA nanoparticles

Colloidal characterization

The colloidal characterization of the particles was done through measurement of the size distribution and polydispersity index (PDI) using dynamic light scattering (DLS) and morphological characterization was done using atomic force microscopy (AFM).

For DLS measurements, a 2 mg/mL suspension of the lyophilized particles was prepared in ultrapure, re-dispersed with a Bioruptor 300 sonication system (Diagenode) (high, 3 cycles, 30 sec ON/10 sec OFF cycle), and analyzed with the Nanotrac Flex (Microtrac). The average of three measurements were used to report the particle size and PDI values.

AFM images were obtained with a Catalyst BioScope (Bruker) coupled to a confocal microscope (TCS SP5II, Leica). 100 μL of 10 mg/mL particle suspension was dried on clean glass substrates and particles were imaged in peak-force tapping mode using a silicon nitride cantilever with nominal spring constant of 0.4 N/m (Bruker). AFM images were analyzed using NanoScope analysis software (Bruker).

Quantification of ESO content

The ESO content of the particles was quantified using UV-Vis spectroscopy. A 10 mg/mL NP suspension was prepared in pH 11 borate buffer, then re-dispersed by sonicating with a Bioruptor 300 sonication system (high, 2 cycles, 30 sec ON/10 sec OFF cycle). The absorbance values were measured on a Nanodrop (2000c, Thermo Scientific). A standard series of ESO in pH 11 borate buffer (1-100 μg/mL) was prepared, and the absorbance values at 301 nm was used to plot a calibration curve. The equation of the curve was used to calculate the amount of ESO in the particles. Then, the encapsulation efficiency (EE) and drug loading (DL) were calculated using the Equations 1 and 2, respectively.

$$\text{Encapsulation efficiency}\ (\%) = \frac{\textit{amount of drug in NPs}}{\textit{total amount of drug used to prepare NPs}} \times 100 \qquad \text{(Equation 1)}$$

$$\text{Drug Loading}\ (\%) = \frac{\textit{amount of drug in NPs}}{\textit{total weight of NPs}} \times 100 \qquad \text{(Equation 2)}$$

Release studies

To study the drug release, a 5 mg/mL NP suspension in PBS was incubated at 37°C with continuous shaking. At several time points (0, 4, 24, and 48 h and day 7, 9, and 14), the suspension was centrifuged at 21'300 × g for 35 min, the supernatant was collected and stored, then the particles were re-suspended in fresh PBS and incubated at 37°C. The released drug was quantified using the calibration curve as mentioned above. To study the release of fluorescent dye, 5 mg/mL NP suspensions prepared in PBS (pH 7.4 and pH

5.8) were incubated at 37°C with continuous shaking. At several time points up to 1 week, the suspension was centrifuged at 21'300 × g for 35 min, the supernatant was collected, then the particles were re-suspended in fresh medium and incubated at 37°C. The fluorescence intensity of the collected supernatants was measured using a fluorescence spectrometer (Perkin Elmer).

In vitro studies

Melanin content measurement

Melanoma cell lines were plated in triplicates for each condition in 6-well plates at 3 × 10^5 cells per well with 2 mL medium. Melanin absorbance was measured at 405 nm (OD405) using a Tecan UV-Vis spectrophotometer. Before measurement, 2.5 × 10^5 cells for each condition were suspended in 250 μL 0.1 N NaOH solution.[6]

NP internalization

For the cellular uptake assessment, we used Atto647-loaded NPs at the concentrations of ESO-loaded NPs. 501 mel, LM56, and LM38 2.5 × 10^5 cells were incubated with 20 μg/mL and 100 μg/mL Atto647-NPs at 37°C and 5% CO_2 atmosphere. Cells were evaluated after 24 h, 48 h and 72 h by flow cytometry using a flow cytometer Cytoflex S and data analyzed with Kaluza software (both Beckman Coulter). For esomeprazole delivery via NPs, melanoma cells (2.5 × 10^5 cells), were preincubated in the presence of 1 μg esomeprazole containing ESO-NPs or the same quantity of empty NPs (eNPs) in 500 μl complete medium for 1 h at 37°C and 5% CO_2 atmosphere, prior to 72 h culture in 2 ml of complete medium. For IFNγ stimulation studies, cells were cultured as described and IFNγ (25 ng/mL) was added for the last 24 h to wells prior to harvesting and evaluation by flow cytometry. Then cells were harvested for evaluation of melanin, acidity of intracellular compartments and phenotype.

LysoSensor, LysoTracker and PD-L1 detection

501 mel, LM56, LM47 and LM38 cells (2.5 × 10^5 cells) were suspended in 200 μL medium and then stained with LysoTracker Red DND-99, which measures the lysosomal activity via accumulation in acidic compartments due to proton trapping, together with LysoSensor Green DND-189 to get information about intracellular acidity, i.e. qualitative analysis of pH in acidic organelles (both Invitrogen) for simultaneous evaluation by flow cytometry. Staining solutions were prepared at 50 nM for LysoTracker and 1 μM for LysoSensor. Cells were incubated at 37°C and 5% CO_2 atmosphere for 30 minutes, then washed and acquired using a flow cytometer Cytoflex S and data analyzed with Kaluza software (both Beckman Coulter). In selected experiments cells were labeled with Anti-PD-L1 (CD274) PE-CF594 (Beckman Coulter) or PC7 (BD Biosciences) conjugated monoclonal antibody for 15 minutes at RT and washed, prior to LysoTracker/LysoSensor staining.

Cell cycle analysis

Melanoma cells were treated for 72 h with eNP, ESO-NP and ESO as described above prior to harvesting. The analysis of the cell cycle was performed by determining the DNA content distribution after propidium iodide staining, using a Cytoflex S and Kaluza software (both Beckman Coulter) according to.[37]

MDSC induction and analysis

Monocytes were isolated from PBMC using the CD14 MicroBeads human (Miltenyi Biotec) and cultured at 37°C and 5% CO_2 atmosphere in RPMI 1640 medium with 10% FBS, L-Glutamine, penicillin and streptomycin in the presence of eNP or ESO-NP (same concentration as for melanoma studies) for 24 h prior to harvesting (patients' MDSCs). From healthy donors' monocytes we generated MDSCs using GM-CSF (40 ng/mL), IL-6 (20 ng/mL), TGFβ (1 ng/mL) for 72 h days prior to incubation with eNP and ESO-NP at the same concentration as for patients' cells and melanoma cell lines for further 24 h. At the end cells were harvested and subjected to flow cytometry analysis. After pre-incubation with Fc blocking agent (Miltenyi Biotec) 10 min at RT, cells were incubated with fluorochrome-conjugated antibodies against HLA-DR, PD-L1, CD14, CD163, CD206, CX3CR1, CD80, CD86 for 20 min at RT before a washing step and acquisition with flow cytometer Cytoflex S and data analyzed with Kaluza software (both Beckman Coulter). The supernatant of co-cultures was recovered and centrifuged at 600 x g for 10 min prior to storage at -80°C for subsequent cytokine detection.

Gene expression analysis

RNA was extracted from melanoma cells with the miRNeasy Mini Kit (QIAGEN), quantified using Nanodrop spectrophotometer (ThermoFisher Scientific), reverse-transcribed using the High-Capacity cDNA Kit, and pre-amplified using a Preamp Master Mix Kit according to the manufacturer's instructions (ThermoFisher Scientific). qRT-PCR was carried out in triplicates and run on QuantStudio 7 Flex instrument and analysis was performed using SDS software QuantStudio 7 Flex software. TaqMan assays for ATP6V1A (Hs01097169_m1), MITF (Hs00165156_m1), HLA-A (Hs01058806_g1), PVR / CD155 (Hs00197846_m1) and TYR (Hs00165976_m1) were used (all purchased from ThermoFisher Scientific).

Cytometric Bead Array

Cytokines (IL-8, IL-6, CCL2) were assessed in cell-free supernatants using a Cytometric Bead Array (CBA) (BD Biosciences), according to the manufacturer's instructions.

QUANTIFICATION AND STATISTICAL ANALYSIS

Statistical analysis was conducted using GraphPad Prism 5 and 8. The data are shown as the mean ± SD or SEM. All experiments were repeated at least three times. The statistical significance and consideration of statistically significant *p* values are indicated in the respective figure legends.